# *Supporting Information*

# Enhancement of the Intrinsic Fluorescence of Acridine and its Induced Circularly Polarized Luminescence (CPL) in Ionic Two-Coordinate Coinage Metal Complexes

Ke-Die Li,[a] Shu-Jia Zheng,[a] Shi-Quan Song,[b] Si-Qi Yu,[a] Yue-Yang Feng,[a] Junzi Liu,[a] You-Xuan Zheng,[b] and Tian-Yi Li*[,a]

[a]. Department of Chemistry, University of Science and Technology Beijing, Beijing, 100083, P. R. China

[b]. School of Chemistry and Chemical Engineering, Nanjing University, Nanjing, 210023, P. R. China

## Table of contents

# General information

All reactants were used directly from commercial sources without additional purification. Anhydrous THF was employed in the synthesis, and all chemical reactions were performed under air atmosphere in oven dried glasswares. The methods of synthesis of MACCuCl (N, N'-bis (diisopropylphenyl) -5,5-dimethyl-4-keto-tetrahydropyrimidin-2-ylidene) -Cu (I) chloride) and MACAgCl (N, N-bis (diisopropylphenyl) -5, 5-dimethyl-4-keto-tetrahydropyrimidin-2-ylidene) -Ag (I) chloride) were referenced from the reported method.[1, 2] All the $^{1}$H NMR and $^{13}$C NMR performed in d-acetone on n a Bruker DPX 400 MHz instrument.

## Synthesis and characterization

**General method:** The carbene-metal-Cl intermediate complex and 1.1 equivalents of acridine were dissolved in 20 mL of THF in a dried 100 mL round-bottom flask. Subsequently, a THF solution containing 1.1 equivalents of AgOTf was added to the mixture. The reaction was stirred for 0.5 hours under ambient air atmosphere at room temperature, resulting in a yellow suspension. After removing the precipitate through a Celite column, the solution was condensed to 2 mL, and the addition of exceed amount of petroleum ether precipitated out the raw product. Recrystallization was performed to purify the raw product, leading to final product as crystalline powders.

**Synthesis of 1 (MAC-Cu-Acridine).** MAC-Cu-Acridine (**1**) was obtained as a yellow solid following the general method. The synthesis involved 250 mg of MACCuCl, 90 mg of acridine, and 132 mg of AgOTf. After recrystallization, the final product yielded over 93%. $^{1}$H NMR (400 MHz, Acetone) δ 9.48 (s, 1H), 8.26 (t, 2H), 7.95-7.85 (m, *J*=15.1, 7.5 Hz, 2H), 7.77-7.63 (m, 8H), 6.22 (t, *J*=18.5 Hz, 2H), 4.47 (s, 2H), 3.64 (setp, *J*=6.8 Hz, 2H), 3.38 (setp, *J*=6.8 Hz, 2H), 1.72 (s, 6H), 1.46 (d, *J*=6.8 Hz, 6H), 1.31-1.23 (m, *J*=13.2, 6.5 Hz, 18H). $^{13}$C NMR (101 MHz, Acetone) δ 141.03, 136.92, 135.90, 132.71, 132.25, 127.29, 127.11, 62.43, 39.22, 25.60, 24.84, 24.74, 24.67, 24.38. MALDI-TOF m/z$^{+}$ calculated for $C_{43}H_{51}CuN_3O^{+}$ as 688.33, found 688.20.

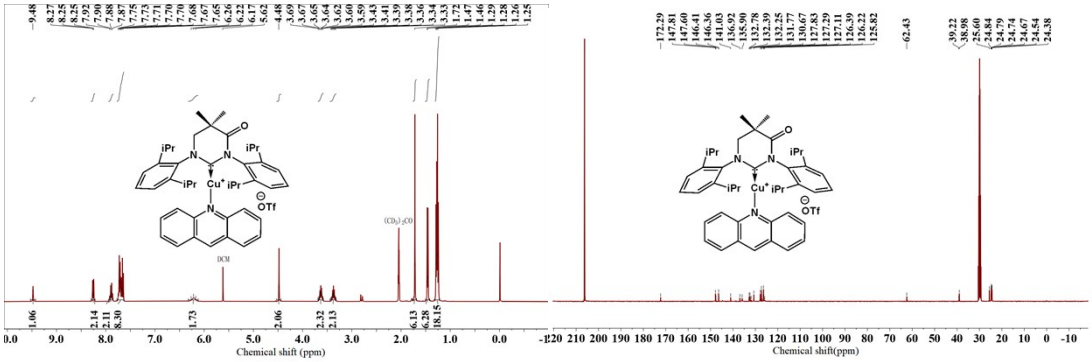

**Figure S1.** $^{1}$H NMR and $^{13}$C NMR spectra of complex **1.**

**Synthesis of 2 (MAC-Ag-Acridine).** MAC-Ag-Acridine (**2**) was obtained as a white solid using a general method. The synthesis utilized 250 mg of MACAgCl, 84 mg of acridine, and 122 mg of AgOTf. After recrystallization, the final product yield exceeded 92%. $^{1}$H NMR (400 MHz, Acetone) δ 9.43 (s, 1H), 8.27 (d, *J*=8.4 Hz, 3H), 7.86 (d, *J*=1.2 Hz, 1H), 7.84 (t, 1H), 7.82 (d, *J* = 1.2 Hz, 1H), 7.74-7.62 (m, 6H), 6.75 (d, *J* = 8.3 Hz, 2H), 4.55 (s, 2H), 3.63 (sept, *J*=6.8 Hz, 2H), 3.37 (sept, *J*=6.8 Hz, 2H), 1.74 (s, 6H), 1.46 (d, *J*=6.8 Hz, 6H), 1.33-1.25 (m, 18H). $^{13}$C NMR (101 MHz, Acetone) δ 149.10, 148.08, 146.84, 143.47, 142.87, 139.26, 135.50, 132.72, 132.23, 130.87, 128.57, 128.32, 128.14, 127.58, 126.70, 62.47, 62.40, 39.70, 30.97, 30.78, 30.59, 30.39, 30.20, 30.01, 29.92, 27.79, 26.03, 25.33, 25.22, 25.13, 24.67. MALDI-TOF *m/z*$^{+}$ calculated for $C_{43}H_{51}AgN_3O^{+}$ as 732.31, found 732.23.

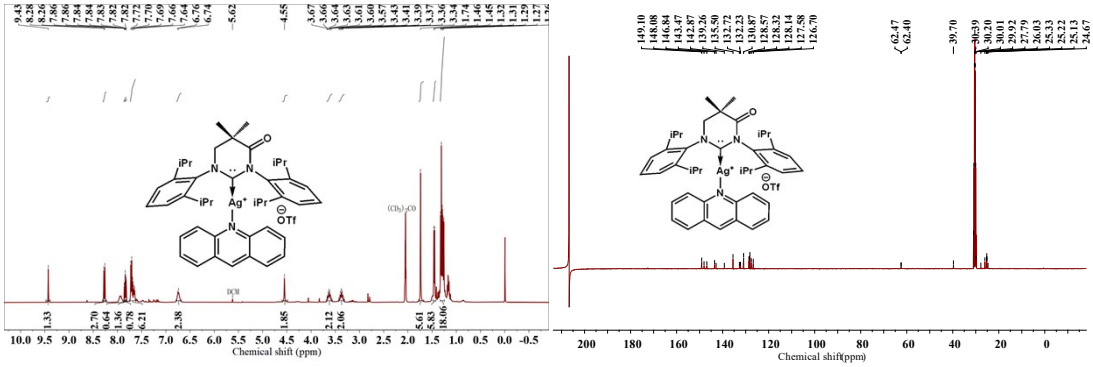

**Figure S2.** $^{1}$H NMR and $^{13}$C NMR spectra of complex **2.**

**Synthesis of 3 (SIPr-Cu-Acridine).** SIPr-Cu-Acridine (**3**) was a white solid taking 250 mg SIPrCuCl, 84 mg acridine and 122 mg AgOTf, after recrystallization the yield of the final production over 88%. $^{1}$H NMR (400 MHz, Acetone) δ 9.50 (s, 1H), 8.28 (d, *J* = 8.4 Hz, 2H), 7.86 (t, *J* = 7.8 Hz, 2H), 7.71-7.59 (m, 8H), 6.65 (d, *J* = 8.7 Hz, 2H), 4.61 (d, *J* = 8.6 Hz, 4H), 3.49 (sept, *J* = 6.9 Hz, 4H), 1.42 (d, *J* = 6.9 Hz, 12H), 1.28 (d, *J* = 6.8 Hz, 12H). $^{13}$C NMR (101 MHz, Acetone) δ 149.41, 149.29, 144.73, 136.27, 135.89, 132.12, 131.25, 128.57, 128.45, 126.70, 126.48, 126.36, 124.76, 121.56, 55.71, 31.07, 30.88, 26.57, 26.39, 25.16, 24.86. MALDI-TOF *m/z*$^{+}$ calculated for $C_{40}H_{47}CuN_3^{+}$ as 632.31, found 632.28.

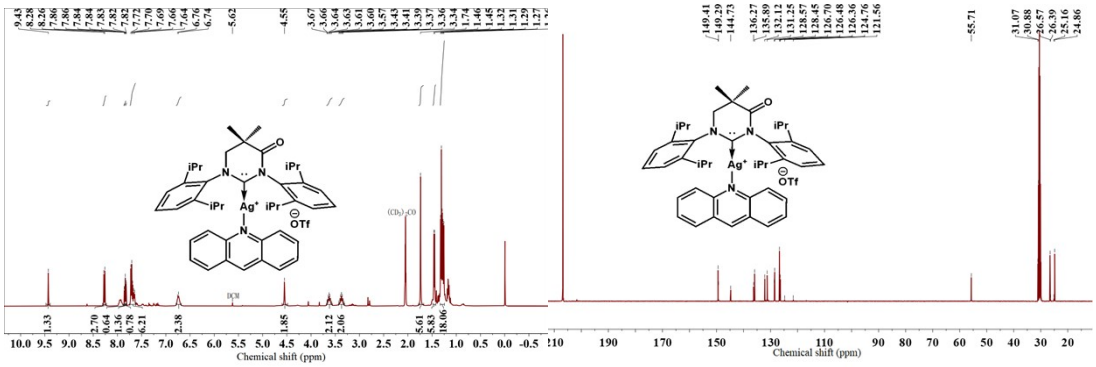

**Figure S3.** $^{1}$H NMR and $^{13}$C NMR spectra of complex **3**.

**Synthesis of MAC-Cu-Acridine (±CS$^{-}$)**. The chiral salt, silver camphor-10-sulfonate (±AgCS), was obtained following the documented procedure.[4] The difference in the synthesis of complex **3** compared to the above method is the use of solution. In this method, we used a mixture of methanol and acetonitrile in a 1:1 volume ratio ($CH_3OH$:MeCN = 1:1) to replace THF, resulting in the formation of complexes **4** and **5** as yellow solids. The reaction employed 250 mg of MACCuCl, 90 mg of acridine, and 171 mg of ±AgCS, yielding 380 mg of the final product with a yield of 90%. $^{13}$C NMR for both complexes can not be obtained owing to their low solubility in most deuterated solvents. For **4**: $^{1}$H NMR (400 MHz, Acetone) δ 9.12 (s, 1H), 8.18 (d, $J$ = 8.4 Hz, 2H), 7.82 (t, $J$ = 6.7 Hz, 3H), 7.70-7.05 (m, 17H), 4.18 (s, 5H), 3.39 (setp, 5H), 3.14 (sept, 5H), 2.89 (d, $J$ = 63.6 Hz, 3H), 2.69-2.14 (m, 4H), 2.00-1.72 (m, $J$ = 57.0, 24.9, 11.2 Hz, 4H), 1.60 (s, 13H), 1.55-1.40 (m, 2H), 1.27 (d, $J$ = 12.0 Hz, 2H), 1.12 – 0.70 (m, $J$ = 97.8 Hz, 8H). MALDI-TOF $m/z^{+}$ calculated for $C_{43}H_{51}CuN_3O^{+}$ as 688.33, found 688.40. For **5**: $^{1}$H NMR (400 MHz, Acetone) δ 9.15 (s, 1H), 8.20 (d, 2H), 7.89-7.31 (m, 12H), 4.25 (s, 2H), 3.43 (sept, 2H), 3.18 (sept, 2H), 2.84 (d, J = 46.7 Hz, 2H), 2.61-2.09 (m, J = 60.7, 21.1, 8.7 Hz, 3H), 1.99-1.66 (m, 3H), 1.62 (s, 5H), 1.42 (d, J = 6.8 Hz, 1H), 1.40-1.29 (m, J = 20.7, 6.4 Hz, 17H), 1.23 (d, J = 6.8 Hz, 1H), 1.19 (d, J = 6.8 Hz, 6H), 1.07-0.64 (m, 4H). MALDI-TOF $m/z^{+}$ calculated for $C_{43}H_{51}CuN_3O^{+}$ as 688.33, found 688.40.

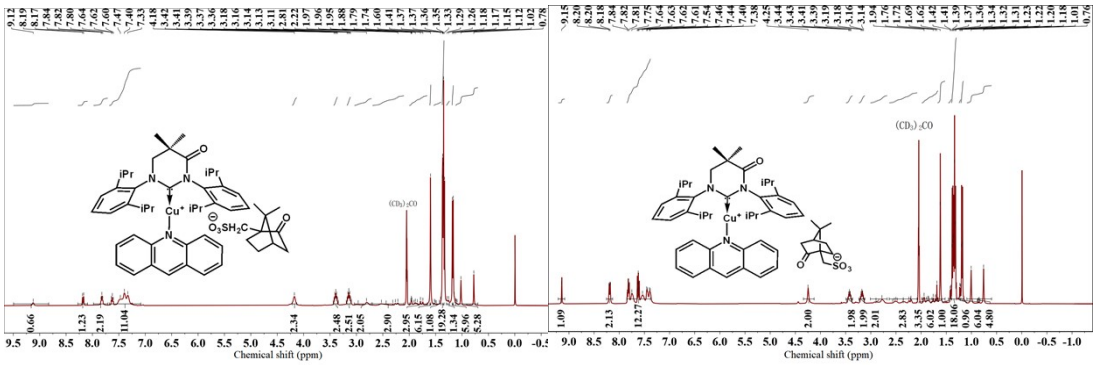

**Figure S4.** $^{1}$H NMR spectra of complex **4** and **5**

## Crystallographic data

All the single crystals of complexes in this work involved were obtained by diffusing diethyl ethyl into $CH_2Cl_2$ solution of the complexes. Paraffin oil was used to select a suitable single crystal under a microscope, and obtained diffraction intensity frames on a Rigaku GeminiE diffractometer using $M_O$ Kα radiation (λ=0.71073 Å) at room temperature. All the ORTEP diagrams were drawn with 50% probability.

**Table S1.** Critical crystallographic data of **1**

| Bond length (Å) | | |
|---|---|---|
| C1-Cu | 1.895(4) | |
| Cu-N1 | 1.914(4) | |
| Bond angle (°) | | |
| N2-C1-Cu | 121.3(3) | ∑=360 |
| N3-C1-Cu | 123.0(3) | |
| N2-C1-N3 | 115.7(4) | |
| Cu-N1-C2 | 121.2(3) | ∑=360 |
| Cu-N1-C3 | 120.2(3) | |
| C2-N1-C3 | 118.6(4) | |
| C1-Cu-N1 | 178.06(16) | |
| Dihedral angle (°) | | |
| N3-C1-N1-C3 | 3.14401 | |
| N2-C1-N1-C2 | 2.50104 | |
| Space group | | |
| (MAC)Cu(Acridine) | $P2_1/c$ | |

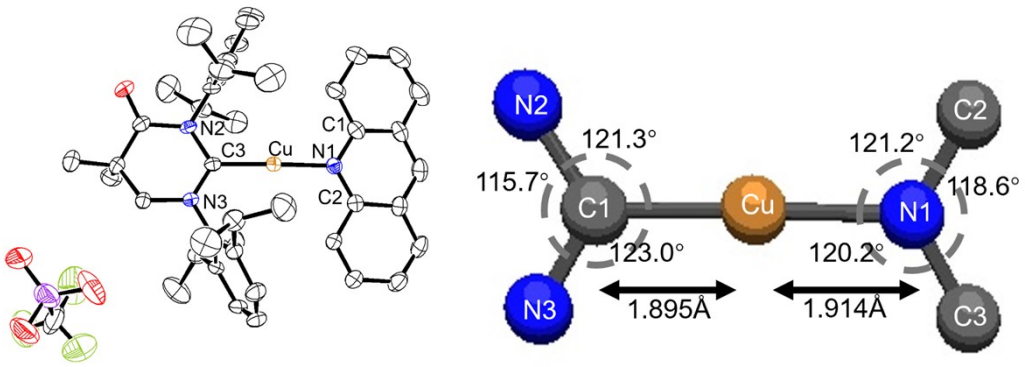


**Figure S5. ORTEP diagram (left) and core structure (right) of 1.**

**Table S2.** Critical crystallographic data of **2**

| Bond length (Å) | | |
|---|---|---|
| C1-Ag | 2.081(4) | |
| Ag-N1 | 2.135(4) | |
| Bond angle (°) | | |
| N2-C1-Ag | 121.5(3) | ∑=360 |
| N3-C1-Ag | 122.0(3) | |
| N2-C1-N3 | 116.5(4) | |
| Ag-N1-C2 | 120.5(4) | ∑=360 |
| Ag-N1-C3 | 119.7(3) | |
| C2-N1-C3 | 119.8(4) | |
| C1-Ag-N1 | 177.35(16) | |
| Dihedral angle (°) | | |
| N3-C1-N1-C3 | 4.06852 | |
| N2-C1-N1-C2 | 0.27250 | |
| Space group | | |
| (MAC)Ag(Acridine) | $P2_1/c$ | |

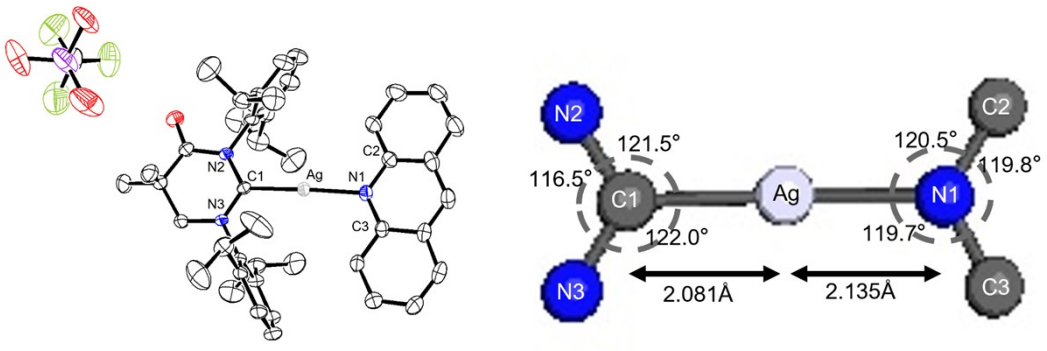


**Figure S6.** ORTEP diagram (left) and core structure (right) of **2**.

**Table S3.** Critical crystallographic data of **3**

| Bond length (Å) | | |
|---|---|---|
| C1-Cu | 1.869(6) | |
| Cu-N1 | 1.902(5) | |
| Bond angle (°) | | |
| N2-C1-Cu | 125.5(4) | ∑=360 |
| N3-C1-Cu | 125.8(4) | |
| N2-C1-N3 | 108.7(5) | |
| Cu-N1-C2 | 121.7(4) | ∑=359.9 |
| Cu-N1-C3 | 120.3(4) | |
| C2-N1-C3 | 117.9(5) | |
| C1-Cu-N1 | 177.2(2) | |
| Dihedral angle (°) | | |
| N3-C1-N1-C3 | 0.54559 | |
| Space group | | |
| (SIPr)Cu(Acridine) | C2/c | |

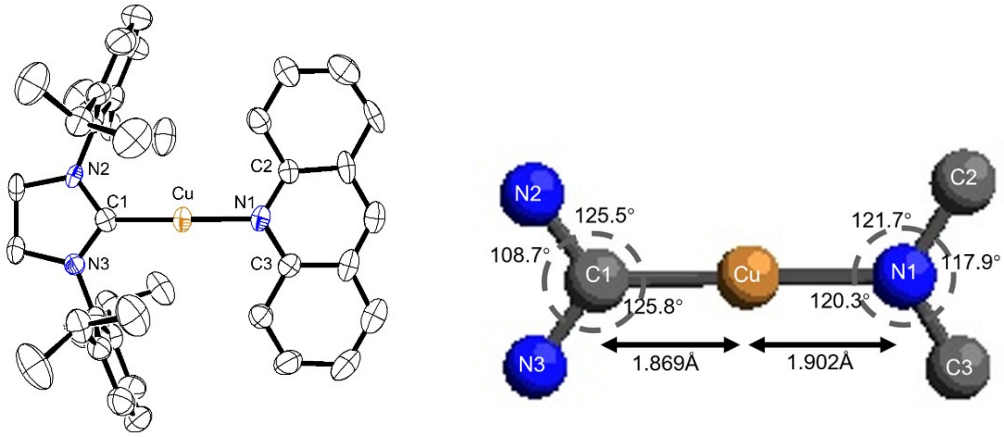


**Figure S7.** ORTEP diagram (left) and core structure (right) of **3**.

**Table S4.** Critical crystallographic data of **4**

| Bond length (Å) | | |
|---|---|---|
| C1-Cu | 1.941(2) | |
| Cu-N1 | 1.941(2) | |
| Bond angle (°) | | |
| N2-C1-Cu | 121.4(3) | ∑=359.9 |
| N3-C1-Cu | 121.7(3) | |
| N2-C1-N3 | 116.8(2) | |
| Cu-N1-C2 | 120.7(3) | ∑=359.9 |
| Cu-N1-C3 | 120.0(3) | |
| C2-N1-C3 | 119.2(2) | |
| C1-Cu-N1 | 178.91(16) | |
| Dihedral angle (°) | | |
| N3-C1-N1-C3 | 1.91473 | |
| N2-C1-N1-C2 | 3.21831 | |
| Space group | | |
| (MAC)Cu(Acridine) $CS^-$ | $P2_12_12_1$ | |

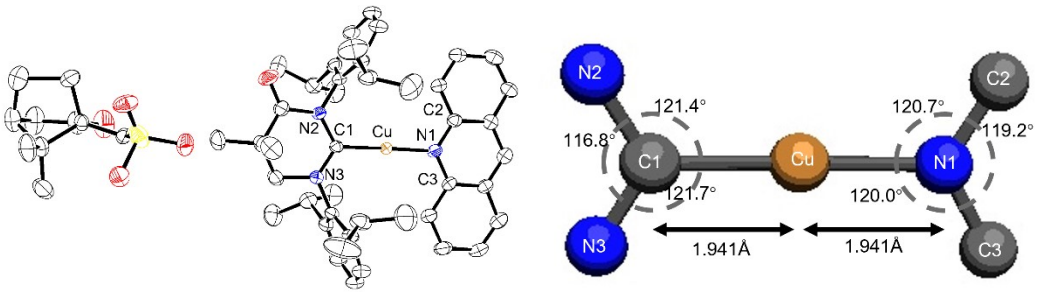


**Figure S8.** ORTEP diagram (left) and core structure (right) of **4**.

**Table S5.** Crystallographic data of **1** to **4.**

| **complex** | **1** | **2** | **3** | **4** |
|---|---|---|---|---|
| Empirical formula | $C_{44}H_{51}CuF_3N_3O_4S$ | $C_{44}H_{51}AgF_3N_3O_4S$ | $C_{40}H_{47}CuN_3$ | $C_{53}H_{66}CuN_3O_5S$ |
| Formula weight | 838.47 | 882.8 | 633.34 | 920.68 |
| Temperature/K | 293(2) | 293 | 293 | 293(2) |
| Crystal system | monoclinic | monoclinic | monoclinic | orthorhombic |
| Space group | $P2_1/c$ | $P2_1/c$ | C2/c | $P2_12_12_1$ |
| a/Å | 14.6647(8) | 14.6167(9) | 22.458(3) | 9.6189(2) |
| b/Å | 20.3416(7) | 20.2723(9) | 15.8230(16) | 16.6313(4) |
| c/Å | 15.7415(7) | 16.0177(7) | 28.556(4) | 30.6506(8) |
| α/° | 90 | 90 | 90 | 90 |
| β/° | 92.666(4) | 90.579(4) | 113.056(15) | 90 |
| γ/° | 90 | 90 | 90 | 90 |
| Volume/Å$^3$ | 4690.7(4) | 4746.0(4) | 9337(2) | 4903.3(2) |
| Z | 4 | 4 | 8 | 4 |
| $\rho_{calc}$g/cm$^3$ | 1.187 | 1.236 | 0.901 | 1.247 |
| μ/mm$^{-1}$ | 0.562 | 0.52 | 0.491 | 0.537 |
| F(000) | 1760 | 1832 | 2696 | 1960 |
| Crystal size/mm$^3$ | 0.8 × 0.6 × 0.1 | 0.8 × 0.6 × 0.1 | 0.6 × 0.1 × 0.1 | 0.17 × 0.16 × 0.1 |
| Radiation | $M_o$ Kα (λ = 0.71073) | $M_o$ Kα (λ = 0.71073) | $M_o$ Kα (λ = 0.71073) | $M_o$ Kα (λ = 0.71073) |
| 2Θ range for data collection/° | 7.022 to 58.532 | 6.874 to 58.85 | 7.026 to 58.462 | 6.798 to 58.4 |
| Index ranges | -18 ≤ h ≤ 19<br>-26 ≤ k ≤ 27<br>-19 ≤ l ≤ 19 | -19 ≤ h ≤ 19<br>-27 ≤ k ≤ 26<br>-22 ≤ l ≤ 19 | -28 ≤ h ≤ 28<br>-21 ≤ k ≤ 20<br>-35 ≤ l ≤ 36 | -13 ≤ h ≤ 11<br>-22 ≤ k ≤ 19<br>-31 ≤ l ≤ 38 |
| Reflections collected | 31996 | 33013 | 28103 | 21556 |
| Independent reflections | 10864 [$R_{int}$ = 0.0481, $R_{sigma}$ = 0.0721] | 11299 [$R_{int}$ = 0.0431, $R_{sigma}$ = 0.0652] | 10716 [$R_{int}$ = 0.1123, $R_{sigma}$ = 0.1569] | 11120 [$R_{int}$ = 0.0153, $R_{sigma}$ = 0.0266] |
| Data/restraints/parameters | 10864/0/515 | 11299/0/515 | 10716/0/405 | 11120/326/750 |
| Goodness-of-fit on $F^2$ | 1.025 | 1.048 | 1.000 | 1.04 |
| Final R indexes [I>=2σ (I)] | $R_1$ = 0.0850, $wR_2$ = 0.2382 | $R_1$ = 0.0683, $wR_2$ = 0.1853 | $R_1$ = 0.1116, $wR_2$ = 0.2945 | $R_1$ = 0.0392, $wR_2$ = 0.0969 |
| Final R indexes [all data] | $R_1$ = 0.1469, $wR_2$ = 0.2833 | $R_1$ = 0.1114, $wR_2$ = 0.2091 | $R_1$ = 0.2144, $wR_2$ = 0.3731 | $R_1$ = 0.0554, $wR_2$ = 0.1064 |
| Largest diff. peak/hole / e Å$^{-3}$ | 0.73/-0.72 | 0.79/-0.73 | 0.71/-0.59 | 0.45/-0.25 |
| Flack parameter | - | - | - | 0.069(16) |

## Electrochemical studies

Cyclic voltammetry (CV) curves were investigated using a PARSTAT 4000A potentiostat galvanostat EIS analyzer in N, N-Dimethylformamide (DMF) with 0.1 M Tetra n butyl ammonium hexafluorophosphate (TBAHFP) as the supporting electrolyte. The measurements were conducted under a $N_2$ atmosphere employing an internal standard method. In this study, a standard three-electrode system was employed, comprising a glassy carbon plate as the working electrode, a platinum wire as the counter electrode, and a silver wire as the reference electrode. In the internal standard method, a reference is necessary to establish the redox values ($^{V}_{ox}$) and potential values ($^{V}_{red}$) as 0 V for comparison with the values of the complexes. The preferred reference chosen for this purpose was ferrocenium/ferrocene ($Fc/Fe^{2+}$). The gap of the highest occupied molecular orbital (HOMO) and the lowest unoccupied molecular orbital (LUMO) energy levels were calculated according the following equations: $E_{HOMO} = -1.15 \times eV_{ox} - 4.79\ (eV)$; $E_{LUMO} = -1.18 \times eV_{red} - 4.83\ (eV)$.[5]

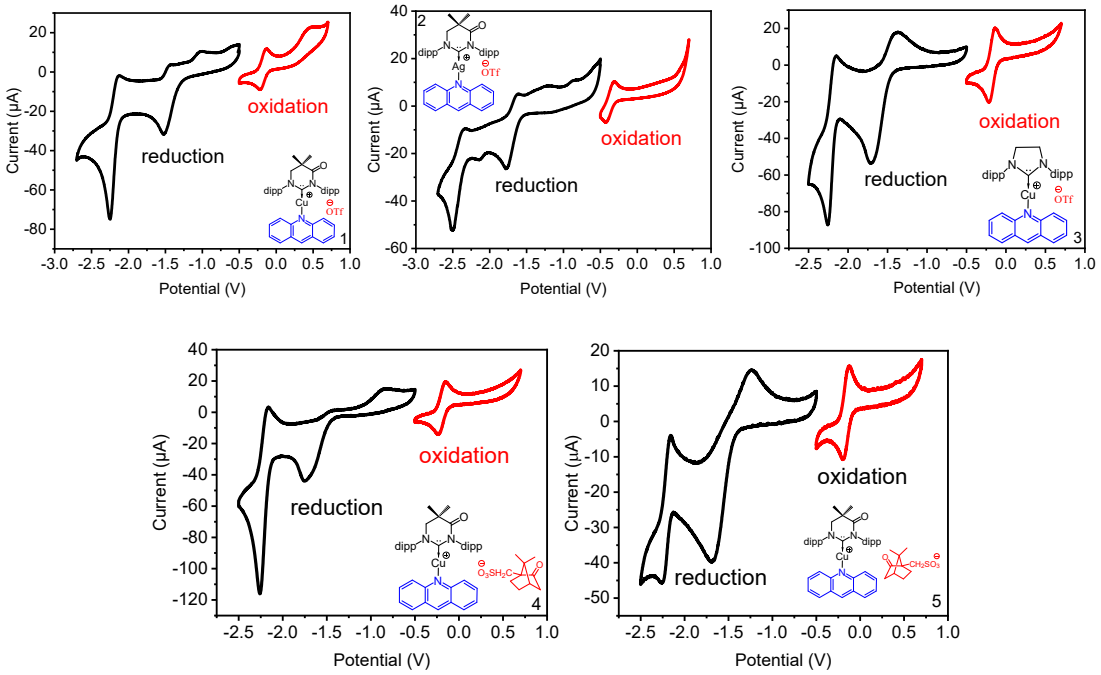


**Figure S9.** CV curves of complexes **1-5.**

## Theoretical calculation

All non-metal atoms in the reported complexes were optimized at the B3LYP/genecp level, with LANL2DZ used for Cu and Ag atoms in their ground states. Time-dependent Density Functional Theory (TDDFT) calculations were conducted using the optimized structures at the CAM-B3LYP/genecp level. These calculations were performed using the Gaussian 09 software package. Natural transition orbitals (NTOs) of complex 1 was shown in the **Table S8**. NTO analysis and visualization were done using Multiwfn and IQmol software.[6]

**Table S6.** HOMO and LUMO plots of **1-3.**

| **Complex** | **1** | **2** | **3** |
|---|---|---|---|
| **HOMO** | 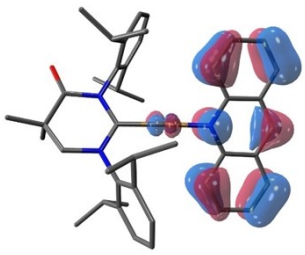 -8.59 eV | 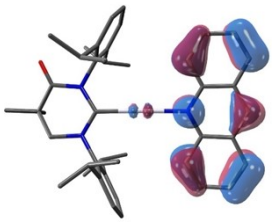 -8.54 eV | 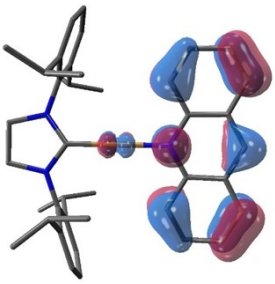 -8.59 eV |
| **LUMO** | 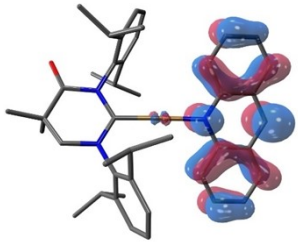 -5.05 eV | 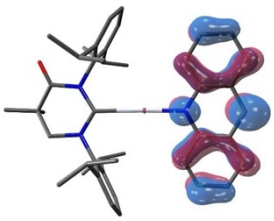 -4.96 eV | 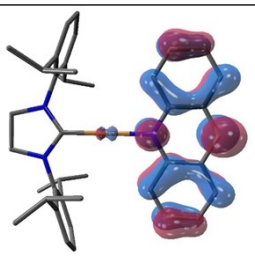 -5.04 eV |

**Table S7.** TD-DFT calculations of **1-3**.

| complex | State | Energy (eV/nm) | Osc. strength | Major contribution |
|---|---|---|---|---|
| **1** | $S_1$ | 3.50/354 | 0.1159 | H → L 96.8% |
| | $T_1$ | 1.76/703 | 0.0000 | H → L 92.3% |
| | $T_2$ | 3.05/405 | 0.0000 | H-4 → L 47.3%<br>H-7 → L 22.9%<br>H → L+6 11.1% |
| **2** | $S_1$ | 3.17/391 | 0.0997 | H → L 97.7% |
| | $T_1$ | 1.92/647 | 0.0000 | H → L 95.4% |
| | $T_2$ | 3.10/400 | 0.0000 | H-5 → L 63.5%<br>H-7 → L 19.5%<br>H → L+6 6.1% |
| | $T_3$ | 3.27/380 | 0.0000 | H-7 → L 50.8%<br>H-5 → L 30.9%<br>H → L+6 9.1% |
| **3** | $S_1$ | 3.13/396 | 0.0790 | H → L 97.8% |
| | $T_1$ | 1.90/653 | 0.0000 | H → L 96.0% |
| | $T_2$ | 3.08/403 | 0.0000 | H-6 → L 68.1%<br>H-8 → L 17.9%<br>H → L+4 7.1% |
| | $T_3$ | 3.25/381 | 0.0000 | H-8 → L 54.0%<br>H-6 → L 27.8%<br>H → L+4 11.9% |

**Table S8.** NTO analysis of **1**.

| complex | $S_1$ | $T_1$ | $T_2$ | $T_3$ |
|---|---|---|---|---|
| **1** | 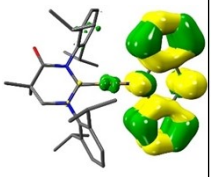 | 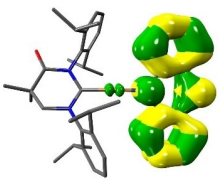 | 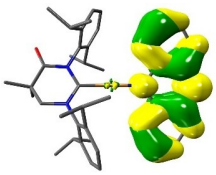 | 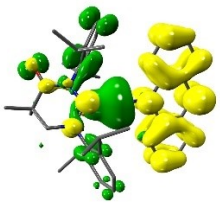 |
| | $^1$LE / MLCT (98.7%) | $^3$LE (97.7%) | $^3$LE (90.1%) | $^3$ICT(96.8%) |
| The green plot represents the hole NTO, while the yellow plot represents the electron NTO. The isosurface value for both hole and electron NTOs is set to 0.030. | | | | |

## Photophysical characterizations

Absorption spectra were recorded using a Techcomp UV-2600 spectrometer from solution ($CH_2Cl_2$ and MeCN) with a concentration of $5\times10^{-5}$ mol/L. Steady-state emission measurements were conducted at room temperature under atmospheric conditions using a HITACHI F-7000 spectrometer, for both solution and crystalline states. Emission lifetimes of all samples and single ligands at room temperature were measured using time-correlated single photon counting (TCSPC) on an Edinburgh FLS 5 spectrometer equipped with an LED excitation source ($\lambda = 375$ nm). Quantum yield measurements of complexes in the crystalline state were carried out using a Hamamatsu C11347-11 absolute PLQY spectrometer equipped with a xenon lamp under a $N_2$ atmosphere. Measurements in the solution state were conducted using the same spectrometer under an air atmosphere.

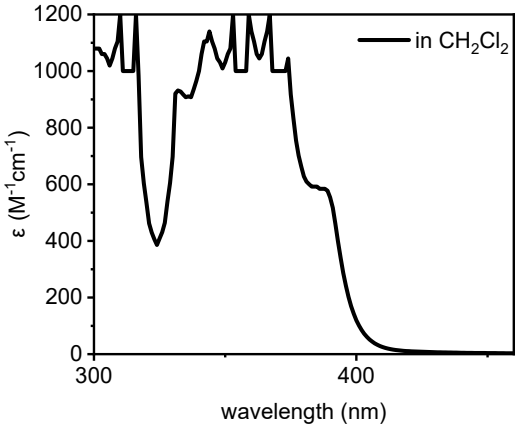


**Figure S10.** Absorption spectra of acridine in concentrated $CH_2Cl_2$ solution.

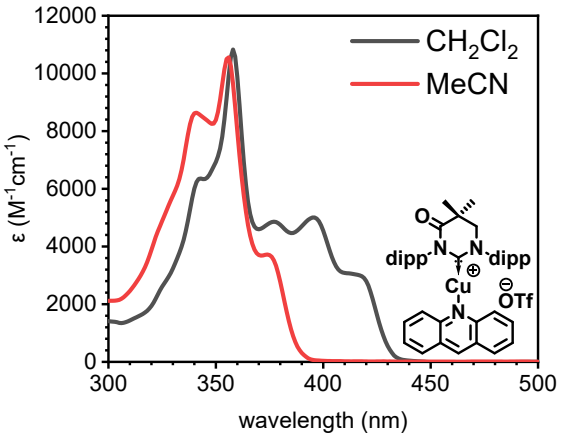


**Figure S11.** Absorption spectra of **1** in $CH_2Cl_2$ and MeCN**.**

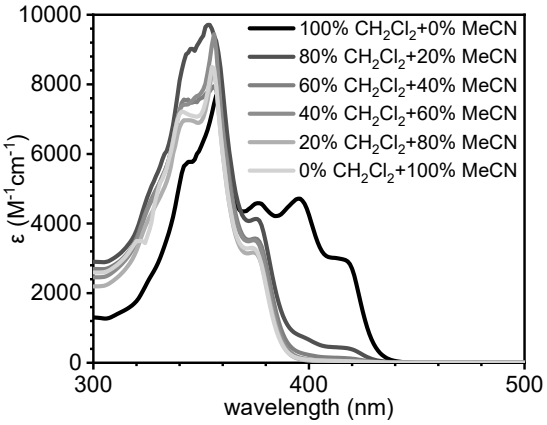


**Figure S12.** Absorption spectra of **1** in mixed solution of $CH_2Cl_2$ and MeCN.

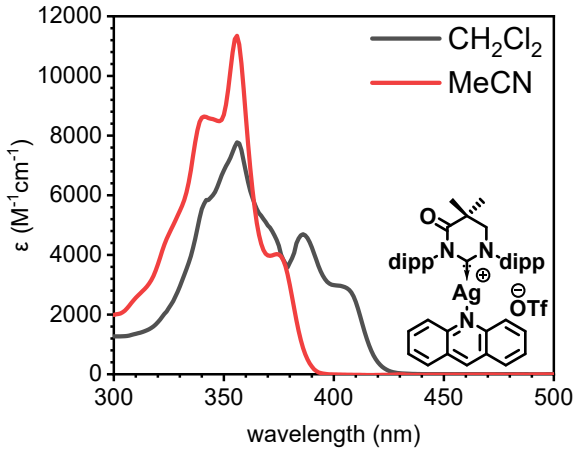


**Figure S13.** Absorption spectra of **2** in $CH_2Cl_2$ and MeCN.

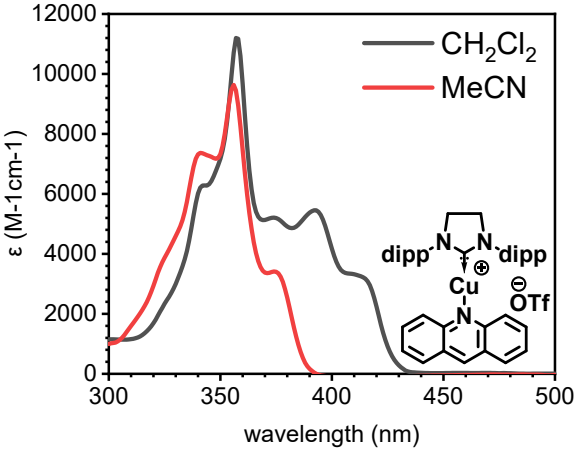


**Figure S14.** Absorption spectra of **3** in $CH_2Cl_2$ and MeCN.

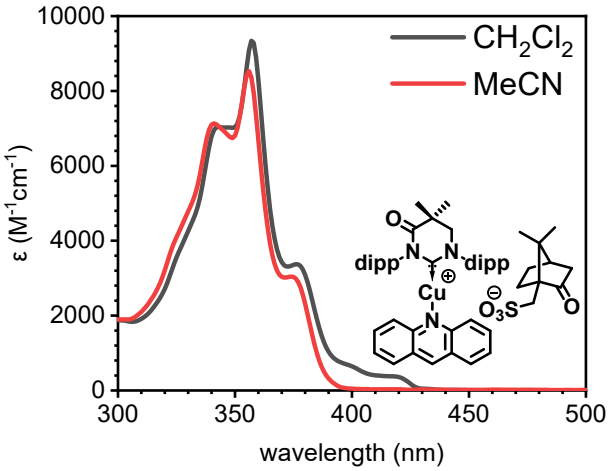


**Figure S15.** Absorption spectra of **4** in $CH_2Cl_2$ and MeCN.

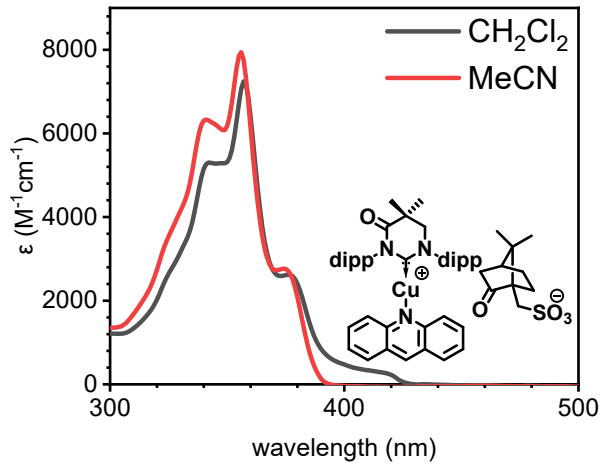


**Figure S16.** Absorption spectra of **5** in $CH_2Cl_2$ and MeCN.

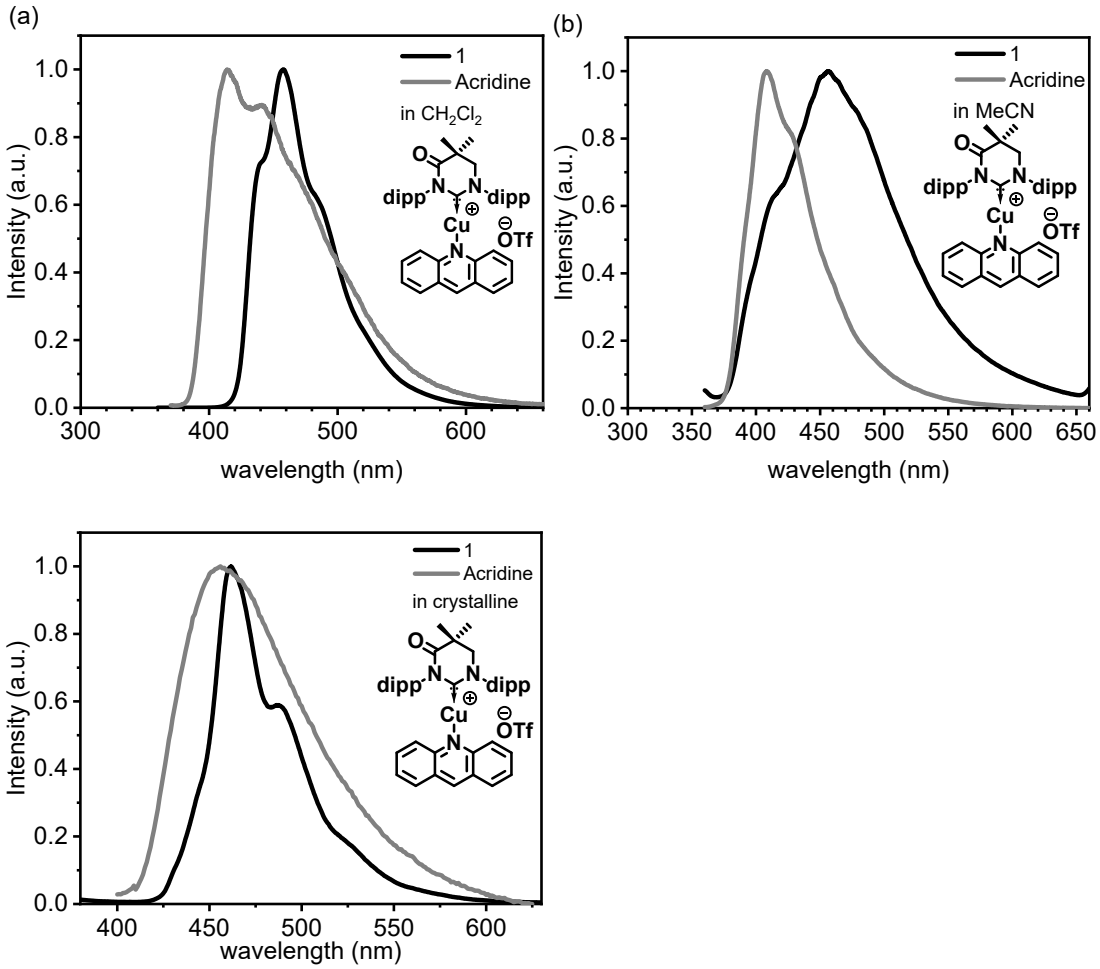


**Figure S17.** Emission spectra of acridine and complex of **1** (a) in $CH_2Cl_2$ (b) in MeCN (c) in crystalline.

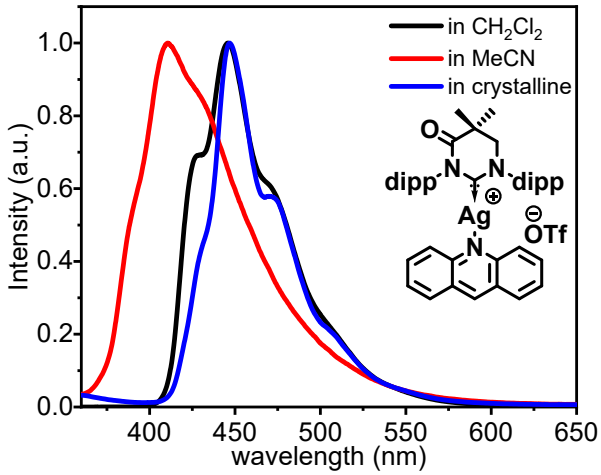


**Figure S18.** Emission spectra of **2** in solution and crystalline**.**

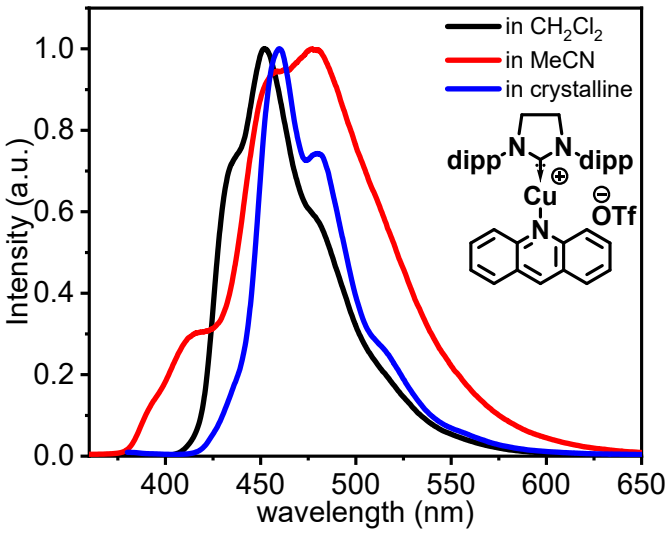


**Figure S19.** Emission spectra of **3** in solution and crystalline.

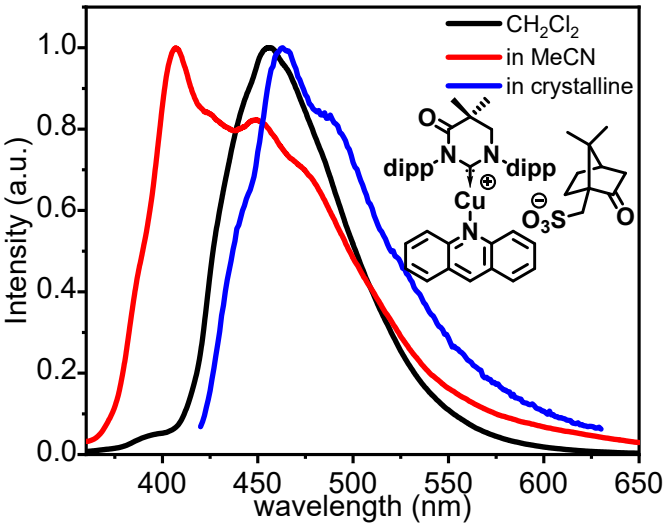


**Figure S20.** Emission spectra of **4** in solution and crystalline.

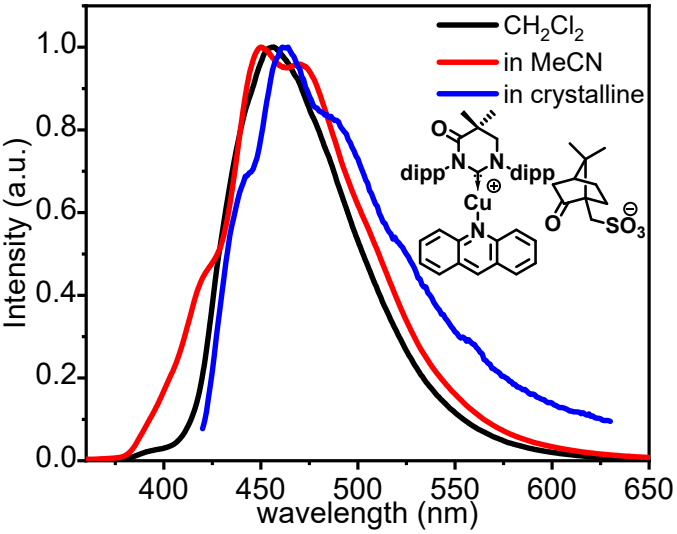


**Figure S21.** Emission spectra of **5** in solution and crystalline.

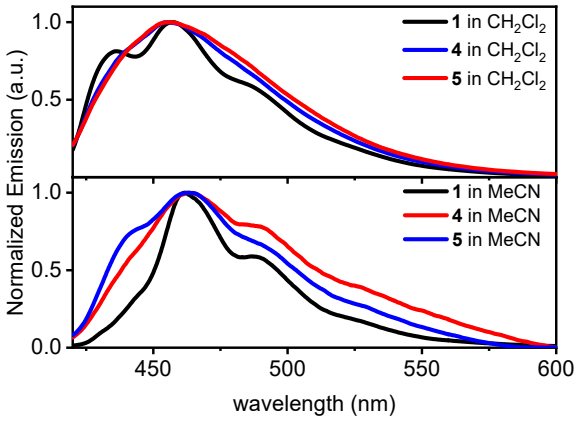


**Figure S22.** Emission spectra of **1**, **4** and **5** in solution.

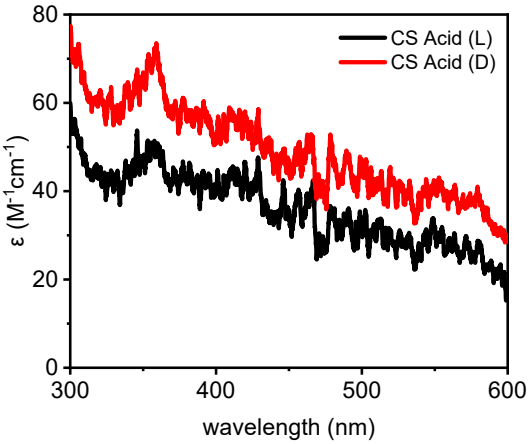


**Figure S23**. Absorption spectra of CS Acid (L/D) in concentrated $CH_2Cl_2$ solution.

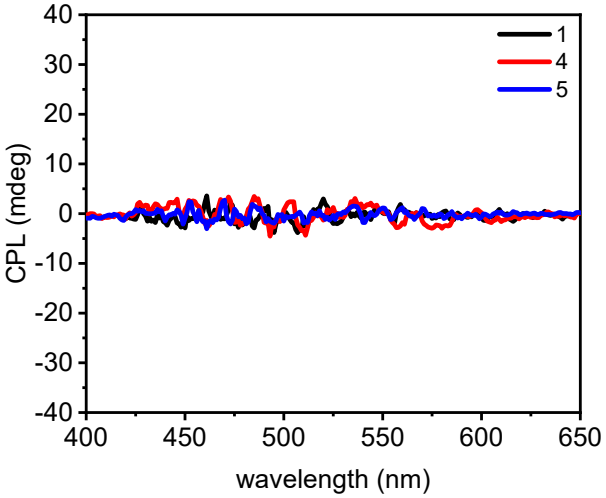


**Figure S24.** CPL spectra of **1**, **4** and **5** in $CH_2Cl_2$.

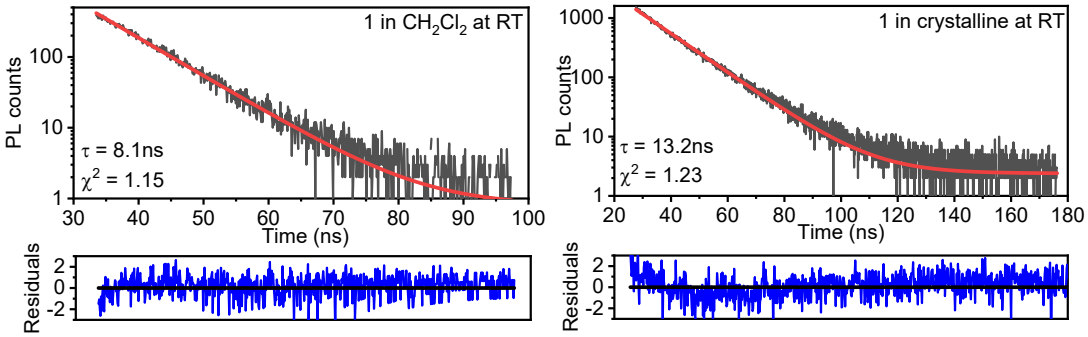


**Figure S25.** Fit of time-resolved emission decay curve of **1** in $CH_2Cl_2$ and crystalline.

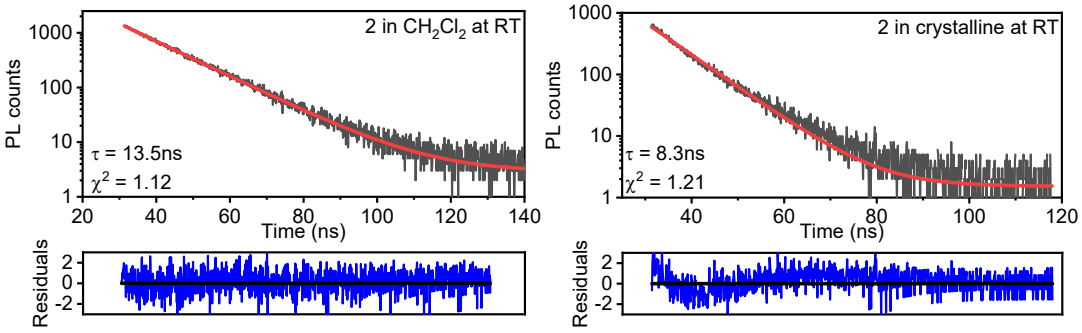


**Figure S26.** Fit of time-resolved emission decay curve of **2** in $CH_2Cl_2$ and crystalline.

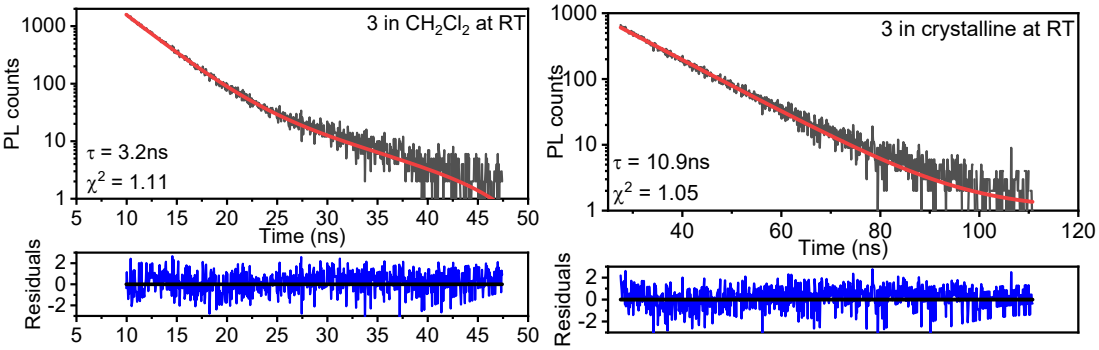


**Figure S27.** Fit of time-resolved emission decay curve of **3** in $CH_2Cl_2$ and crystalline.

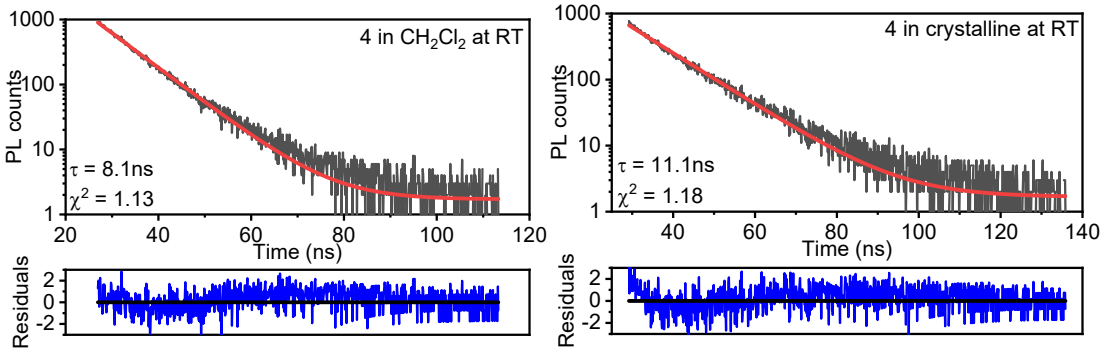


**Figure S28.** Fit of time-resolved emission decay curve of **4** in $CH_2Cl_2$ and crystalline.

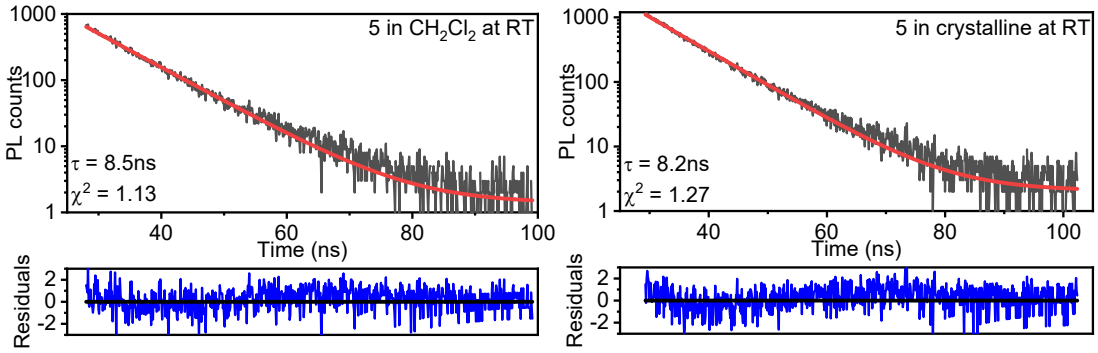


**Figure S29.** Fit of time-resolved emission decay curve of **5** in $CH_2Cl_2$ and crystalline.

## References


1. S. Shi, M. C. Jung, C. Coburn, A. Tadle, D. Sylvinson M. R, P. I. Djurovich, S. R. Forrest and M. E. Thompson, *J. Am. Chem. Soc.*, 2019, **141**, 3576-3588.
2. R. Hamze, S. Shi, S. C. Kapper, D. S. Muthiah Ravinson, L. Estergreen, M.-C. Jung, A. C. Tadle, R. Haiges, P. I. Djurovich, J. L. Peltier, R. Jazzar, G. Bertrand, S. E. Bradforth and M. E. Thompson, *J. Am. Chem. Soc.*, 2019, **141**, 8616-8626.
3. K. Kim and Y. Lee, *The Journal of Organic Chemistry*, 2022, **87**, 569-578.
4. P. A. Krasutskii, V. N. Rodionov, V. P. Tikhonov and A. G. Yurchenko, *Theor. Exp. Chem.*, 1984, **20**, 55-61.
5. G. A. Blake, J. P. Moerdyk and C. W. Bielawski, *Organometallics*, 2012, **31**, 3373-3378.
6. T. Lu and F. Chen, *J. Comput. Chem.*, 2011, **33**, 580-592.